ESMO GOOD SCIENCE BETTER MEDICINE BEST PRACTICE

ANNALS OF ONCOLOGY DRIVING INNOVATION IN ONCOLOGY

ORIGINAL ARTICLE

Longitudinal transcriptomic profiling identifies predictors of response to neoadjuvant chemoimmunotherapy in triple-negative breast cancer: results from the NeoTRIPaPDL1 trial

M. Dugo[1], C.-S. Huang[2], D. Egle[3], B. Bermejo[4], R. S. Seitz[5], T. J. Nielsen[5], C. Zamagni[6], M. Thill[7], A. Antón-Torres[8], S. Russo[9], E. Sevillano[10], E. M. Ciruelos[11], B. L. Schweitzer[5], B. Galbardi[1], R. Greil[12], V. Semiglazov[13], M. Colleoni[14], C. M. Kelly[15,16], L. Del Mastro[17,18], G. Mariani[19], Gi. Viale[1,20], B. Győrffy[21,22,23], H. R. Ali[24,25], L. Pusztai[26], G. Viale[14], M. Callari[27], L. Gianni[27]* & G. Bianchini[1,20]*

[1]Department of Medical Oncology, IRCCS Ospedale San Raffaele, Milan, Italy; [2]Surgery Department, National Taiwan University Hospital, College of Medicine, National Taiwan University and Taiwan Breast Cancer Consortium, Taipei City, Taiwan; [3]Department of Gynaecology, Medical University Innsbruck, Innsbruck, Austria; [4]Department of Medical Oncology, Hospital Clinico Universitario de Valencia, Valencia, Spain; [5]Insight Molecular Diagnostics Inc., Nashville, USA; [6]Medical Oncology Unit, IRCCS Azienda Ospedaliero-Universitaria di Bologna, Bologna, Italy; [7]Gynecology and Gynecological Oncology, Agaplesion Markus Hospital, Frankfurt, Germany; [8]Unit of Medical Oncology, Hospital Universitario Miguel Servet, Zaragoza, Spain; [9]Department of Oncology, Azienda Sanitaria Universitaria Friuli Centrale, Udine, Italy; [10]HM CIOCC MADRID (Centro Integral Oncológico Clara Campal), Laboratorio de Innovación en Oncología, Instituto de Investigación Sanitaria HM Hospitales, Madrid; [11]Servicio Oncologia Médica, University Hospital 12 de Octubre, Madrid, Spain; [12]Department of Internal Medicine III, Paracelsus Medical University, Salzburg, Austria; [13]N. N. Petrov Research Institute of Oncology, St. Petersburg, Russian Federation; [14]IEO, Istituto Europeo di Oncologia IRCCS, Milan, Italy; [15]Department of Medical Oncology, Mater Private Hospital, Dublin; [16]Cancer Trials Ireland, Dublin, Ireland; [17]Clinical Oncology Unit, AOM - IRCCS Ospedale Policlinico San Martino, Genova; [18]Department of Internal Medicine and Medical Specialties, Università di Genova, Genova; [19]Department of Medical Oncology, Fondazione IRCCS Istituto Nazionale dei Tumori, Milan; [20]School of Medicine and Surgery, Università Vita-Salute San Raffaele, Milan, Italy; [21]Department of Bioinformatics, Semmelweis University, Budapest; [22]Institute of Transdisciplinary Discoveries, Medical School, University of Pecs, Pecs; [23]Cancer Biomarker Research Group, Institute of Molecular Life Sciences, HUN-REN Research Centre for Natural Sciences, Budapest, Hungary; [24]CRUK Cambridge Institute, University of Cambridge, Cambridge; [25]Department of Histopathology, Addenbrookes Hospital, Cambridge, UK; [26]Yale Cancer Center, Yale School of Medicine, New Haven, USA; [27]Fondazione Michelangelo, Milan, Italy.

Available online 19 May 2026

Background: Triple-negative breast cancer (TNBC) is immunogenic, but only a subset of patients benefits from neoadjuvant immune checkpoint inhibitors combined with chemotherapy. Predictive biomarkers to guide patient selection and treatment adaptation are lacking.

Patients and methods: In the randomized phase III NeoTRIPaPDL1 trial, 280 patients with high-risk TNBC received neoadjuvant carboplatin plus nab-paclitaxel (CT, $n = 142$) or the same regimen with atezolizumab (CT/A, $n = 138$). Tumor biopsies were collected at baseline and on the first day of the second cycle (D1C2). Longitudinal RNA sequencing was performed to evaluate hallmark, immune, and ferroptosis-related gene signatures. Associations with pathologic complete response (pCR) were assessed using univariable logistic regression and multivariable XGBoost models.

Results: At baseline, in the CT/A arm, higher proliferation and lower stromal and metabolic programs were associated with increased pCR rate. Absence of tumor cells in early on-treatment biopsies strongly predicted surgical pCR in both treatment arms. Comparison of on-treatment with baseline samples revealed a reduced proliferation and increased immune and stromal signatures. These changes were more pronounced in tumors achieving pCR, particularly in patients receiving chemoimmunotherapy. Immune deconvolution analyses confirmed dynamic remodeling of the tumor microenvironment during treatment, with response-associated enrichment of immune cell populations and reduction of tumor epithelial fractions. Although several metabolic signatures were associated with outcome at baseline, most lost predictive value on-treatment, where immune-related programs became the dominant correlates of response. Exploratory multivariable analyses suggested complementary contributions of on-treatment cytotoxic immune activity and iron metabolism in shaping response to chemoimmunotherapy.

*Correspondence to: Dr Giampaolo Bianchini, Department of Medical Oncology, IRCCS Ospedale San Raffaele, via Olgettina 60, Milan 20132, Italy. Tel: +39 02 26436 561

E-mail: bianchini.giampaolo@hsr.it (G. Bianchini).

Dr Luca Gianni, Fondazione Michelangelo, Fondazione Michelangelo, Agostino Bertani 14, Milan 20121, Italy. Tel: +39 02 87086 420

E-mail: luca.gianni@fondazionemichelangelo.org (L. Gianni).

Conclusions: Longitudinal transcriptomic profiling revealed dynamic tumor and microenvironment remodeling during neoadjuvant therapy in TNBC. Baseline tumor-intrinsic features and early treatment-induced immune activation provide complementary information for predicting response to chemoimmunotherapy. Early tumor clearance in on-treatment biopsies represents a strong surrogate of pCR and supports investigation of response-adapted neoadjuvant strategies.

Key words: immunotherapy, longitudinal sampling, neoadjuvant therapy, predictive biomarker, transcriptomic profiling, triple-negative breast cancer

GRAPHICAL ABSTRACT

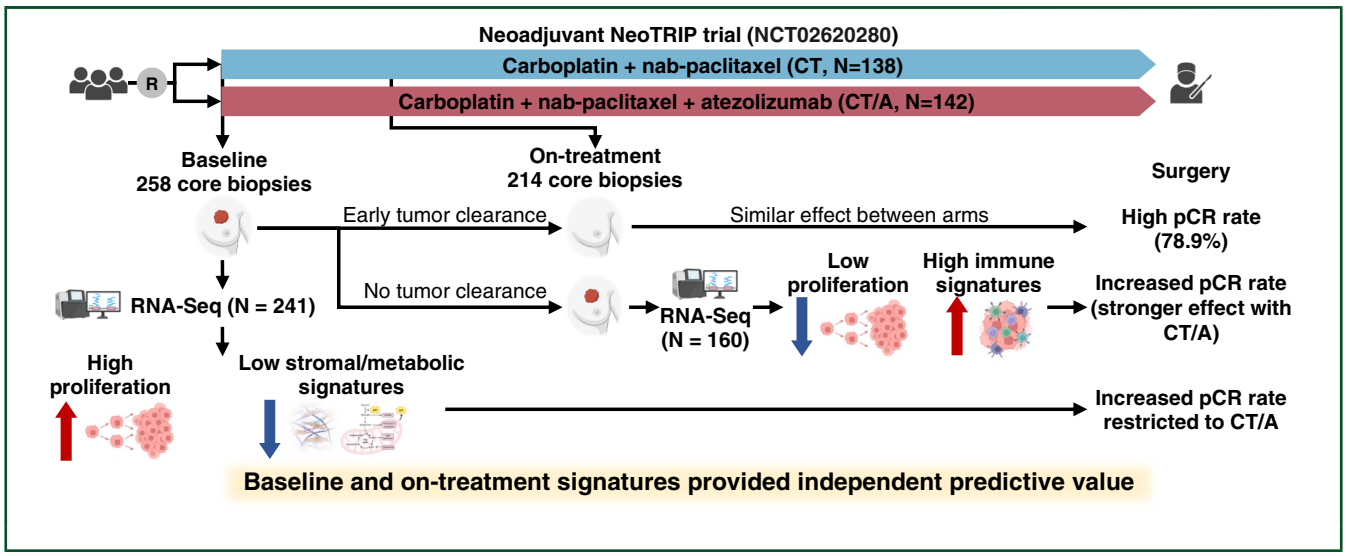

INTRODUCTION

Many features point to triple-negative breast cancer (TNBC) as an immunogenic disease.[1] TNBCs have higher levels of stromal tumor infiltrating lymphocytes (sTILs) and tumor mutational burden compared with luminal tumors,[1-3] and TNBC with high sTILs often show elevated expression of programmed cell death ligand 1 (PD-L1), which mediates tumor escape.[4,5] Immune checkpoint inhibitors (ICIs) reinvigorate the antitumor immune response by blocking the activity of cytotoxic T lymphocyte-associated protein 4, PD-L1, or its receptor, programmed cell death.

Perioperatory pembrolizumab combined with neoadjuvant chemotherapy is the standard of care in intermediate/high-risk TNBC, demonstrating an increased pCR rate, event-free survival, and overall survival.[6,7] However, the benefit is limited to a minority of patients, with many cured by chemotherapy only, and others relapsing despite immunotherapy. Other trials, with the exception of the NeoTRIPaPDL1 trial (NeoTRIP), confirmed the improved benefit from ICIs in combination with neoadjuvant chemotherapy in TNBC.[6,8-12] Considering the potential long-term and irreversible immune-related toxicity of ICIs, and their cost, treatment tailoring to patients who benefit and deserve ICIs is an unmet need. Although no biomarker has yet been clinically validated to guide the use of ICI in early-stage TNBC, several candidate biomarkers have been explored.

High levels of sTILs and PD-L1 are predictive of a higher likelihood of pCR after neoadjuvant chemotherapy with or without concurrent ICI therapy.[6,12-17] However, even cancers with low or absent PD-L1 expression and minimal levels of sTIL have higher pCR and improved EFS when ICI is included with chemotherapy,[6,8] indicating that they do not seem to be useful for tailoring treatments. Several translational studies showed that immune gene signatures reflecting an inflamed tumor microenvironment may be predictive of response to neoadjuvant chemoimmunotherapy in early TNBC.[15-19] However, their ability to specifically predict benefit from the addition of immunotherapy remains heterogeneous across studies. Moreover, most studies evaluating predictive biomarkers for ICI in early TNBC relied on analyses of pre-treatment tumor samples, whereas only a few have included longitudinal tumor sampling during treatment, especially in randomized phase II/III trials.[20-23]

In this study, we investigated whether gene expression analysis of tumor biopsies obtained before and early-on during neoadjuvant chemotherapy and chemoimmunotherapy, as assessed in a phase III randomized trial, NeoTRIPaPDL1, could reveal predictive markers of resistance and sensitivity. We also assessed whether treatment-induced changes could help understand the biology of response and resistance to immunotherapy and might serve as an early surrogate marker of benefit from ICI therapy in TNBC.

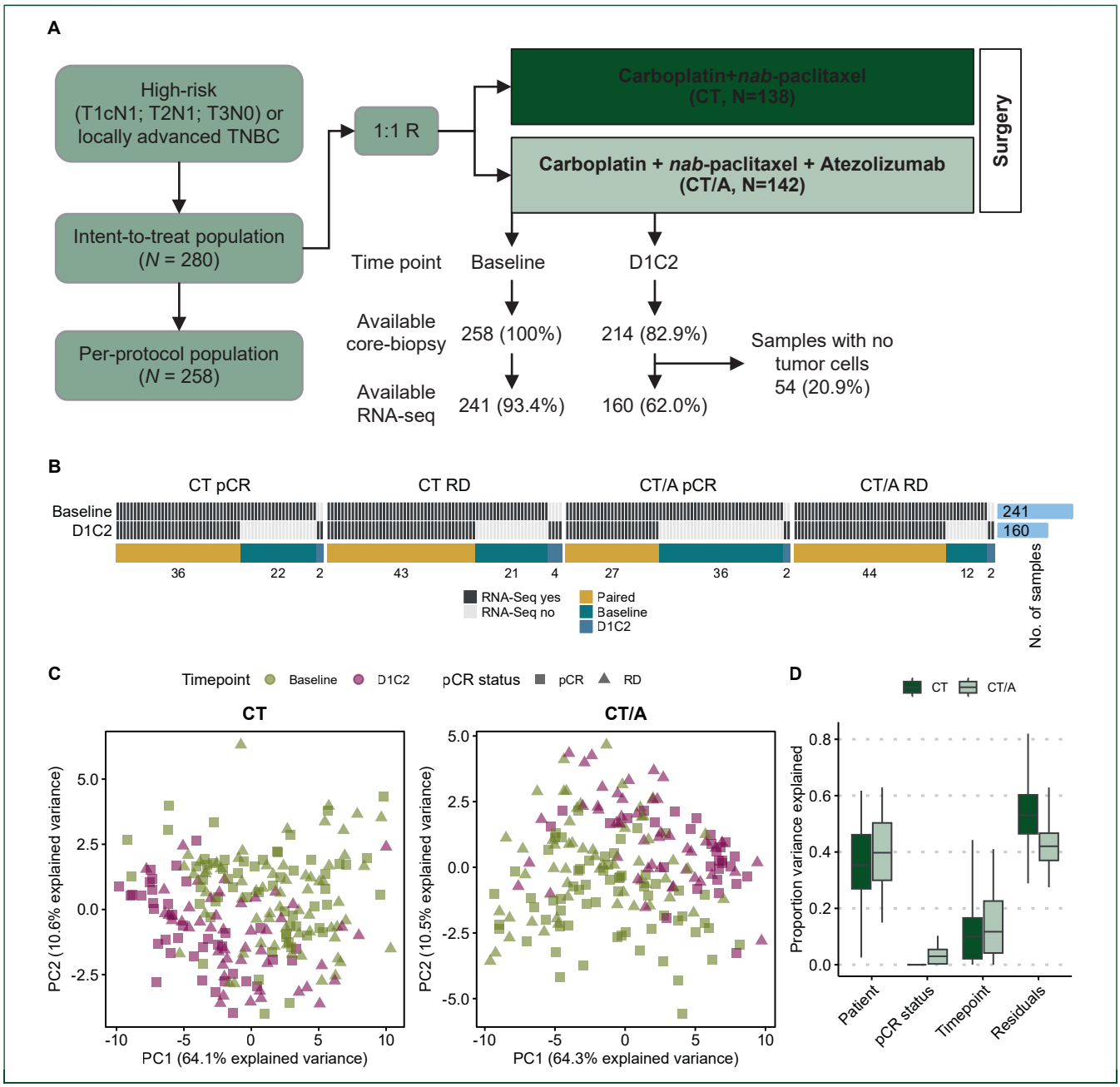

Figure 1. Longitudinal transcriptomic profiling of NeoTRIP tumor samples. (A) Schematic view of the NoeTRIP trial. (B) Availability of baseline and D1C2 RNA-Seq data of tumor samples stratified by arm and pCR status. (C) PCA of baseline and D1C2 tumor samples according to gene signature expression in the two treatment arms. (D) Boxplot of the proportion of variance explained by each variable in each treatment arm.
PC, principal component; PCA, Principal component analysis; pCR, pathologic complete response.

MATERIALS AND METHODS

Patient population and sample collection

NeoTRIP is a multicenter open-label phase III study (NCT02620280) that randomized 280 patients with high-risk TNBC (locally advanced, node positive, and pT3N0) to either neoadjuvant carboplatin and nab-paclitaxel (CT arm, $N = 142$) or to the same chemotherapy concurrent with atezolizumab (CT/A arm, $N = 138$).[24] Both regimens were given every 3 weeks for eight cycles followed by surgery (Figure 1A). Of the 280 patients enrolled in the NeoTRIP study, 258 were evaluable for pathologic complete response at surgery as Per-Protocol Population[24] and only this population was considered for this transcriptomic analysis of tumor samples collected longitudinally during the study. Formalin-fixed paraffin-embedded (FFPE) tumor core biopsies were collected pretreatment and on the first day of the second treatment cycle (D1C2).

The study was undertaken in accordance with Good Clinical Practice guidelines and the Declaration of Helsinki. All patients provided written informed consent. Approvals for the study protocol (and any modifications thereof) were obtained from independent ethics committees at each participating institution and relevant competent authorities.

RNA extraction and sequencing

RNA was extracted from 5 µm FFPE tissue sections of pre- and on-treatment biopsies using the Maxwell RSC RNA FFPE Kit. Exome-enriched libraries were prepared with TruSeq RNA Exome (Illumina) and sequenced on NextSeq 500/2000 with paired-end 75 bp reads. Gene-level transcripts per million (TPM) values were obtained using the Spliced Transcripts Alignment to a Reference (STAR)[25] and the RNA-Seq by Expectation-Maximization (RSEM)[26] software. Processed data are available at National Center for Biotechnology Information (NCBI) Gene Expression Omnibus (GEO) with accession number GSE319641.

Bioinformatics and statistical analyses

Analyses were restricted to the per-protocol population. Single-sample gene signature scores were derived with singscore across 87 signatures, including MSigDB Hallmarks,[27] ConsensusTME immune cell types,[28] and metabolic/ferroptosis gene sets[29] (Supplementary Table S1, available at https://doi.org/10.1016/j.annonc.2026.05.694). Pairwise Pearson correlations were computed between all signature scores, retaining only correlations ≥ 0.8 to construct a similarity network. Gene sets were then annotated into macrocategories by applying the edge betweenness community detection algorithm (Fig. Supplementary Figure S1). Associations with pCR of variables at each time point as well as the delta expression between on- and pretreatment samples were evaluated by logistic regression. Differential expression was analyzed with limma.[30] Bulk RNA-Seq deconvolution was performed with InstaPrism.[31] Multivariable analyses used XGBoost[32] with hyperparameter optimization via 5-fold stratified cross-validation and performance evaluation by 10-fold cross-validation repeated 100 times. All *P* values were corrected by Benjamini-Hochberg false discovery rate (FDR). FDR < 0.05 was considered significant. Additional methodological details are available in Supplementary Methods, available at https://doi.org/10.1016/j.annonc.2026.05.694. Analysis scripts are available at https://github.com/mdugo/Early_GEP_NeoTRIP.

RESULTS

Longitudinal expression profiling of NeoTRIP TNBC patients

Longitudinal RNA-Seq was obtained for 251 of the 258 patients of the per-protocol population: pretreatment (baseline, $N = 241$) and on the first day of the second treatment cycle (D1C2, $N = 160$). Patients without tumor cells on D1C2 ($n = 54$) were excluded from this analysis. For 150 patients, paired baseline and D1C2 RNA-Seq profiles were obtained (Figure 1B). We evaluated expression changes during neoadjuvant treatment and the association with pCR status of gene signatures representative of hallmark biological processes, immune cell subsets, and ferroptosis-related pathways, which have been implicated in immunomodulation in TNBC.[33] Principal component analysis using these signatures showed a major separation of samples according to the timepoint. Samples were instead intermixed according to pCR status (Figure 1C). For each treatment arm, we evaluated the proportion of variance of each gene signature explained by the main variables of the study (Figure 1D). A consistent portion of variability is associated with heterogeneity between patients, followed by variability linked to timepoint. The proportion of variability explained by pCR status was marginal. The largest amount of variability was associated with unknown factors.

Overall, these findings indicate that interpatient heterogeneity and treatment-induced temporal changes are the main drivers of transcriptional variability, whereas differences related to therapeutic response play only a minor role.

Baseline gene signatures associated with response

We compared the baseline signature expression between the two treatment arms. No significant differences were detected; however, baseline samples from the CT arm showed slightly higher expression of immunological signatures than those from the CT/A arm (Supplementary Figure S2, available at https://doi.org/10.1016/j.annonc.2026.05.694). This is in line with our previous observation in this study that baseline sTILs were higher in the CT than the CT/A arm.[14]

Next, we evaluated the association between baseline signatures and pCR using univariate logistic regression for each treatment arm. Although the results were qualitatively similar in the two treatment arms, statistically significant associations (false discovery rate < 0.05) were only observed in the CT/A arm (Figure 2A). Higher pCR rates were associated with high expression of proliferation signatures. Conversely, metabolic, hormonal, signaling, and stromal signatures were associated with lower pCR rates (Figure 2A). There was a significant test of interaction ($P < 0.05$) for seven signatures related to ferroptosis, stroma, and proliferation, indicating a treatment-specific association with response (Figure 2B). Indeed, high proliferation (HM MITOTIC SPINDLE signature) was associated with higher pCR rates in the CT/A arm, but not in the CT arm. High expression of the other six signatures was associated with lower pCR rates only in the CT/A arm (Figure 2B).

Baseline signatures predictive of an early on-treatment pathologic complete response

Among the 251 patients, 225 had an evaluable core biopsy at D1C2. A subset of them ($N = 54$) had no detectable cancer cells in the D1C2 core biopsy (eg, early pathological complete response, early-pCR). This early-pCR occurred more frequently in patients receiving CT/A than in those receiving CT alone (33.6% vs. 16.8%, $P = 0.007$). The absence of tumor cells in the D1C2 core biopsy strongly predicted pCR at surgery, regardless of treatment arm (Figure 3A). The predictive performance of e-pCR for surgical pCR was quantified, yielding a positive predictive value (PPV) of 77.8% (95% CI 52.4%-93.6%) and a negative predictive value (NPV) of 54.4% (95% CI, 43.6%-65.0%) in the CT arm. In the CT/A arm, the PPV and NPV were 80.6% (95% CI

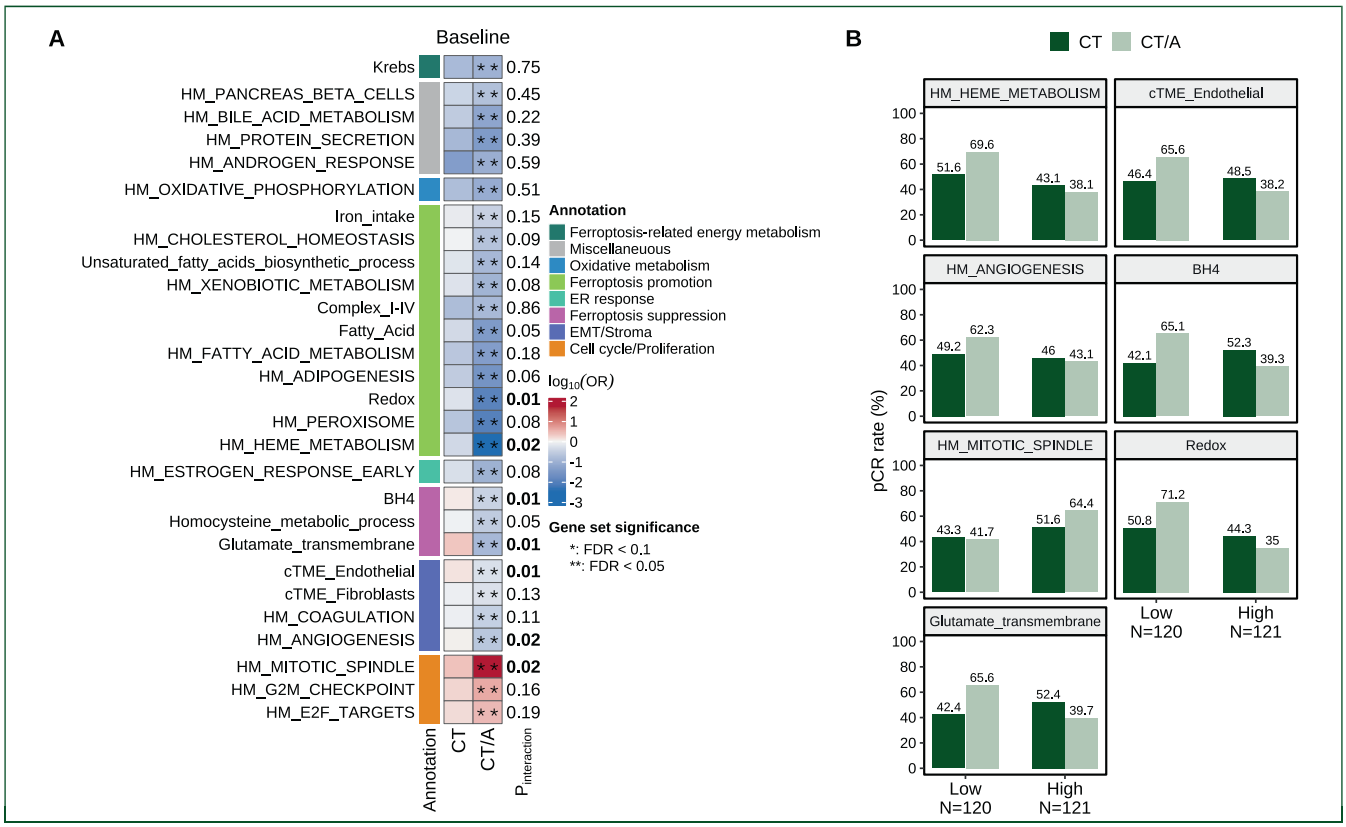

Figure 2. Baseline gene signatures associated with pCR status. (A) The heatmap displays the log OR obtained from univariate logistic regression models. Gene signatures with an FDR < 0.05 in at least one treatment arm are reported. Asterisks indicate the level of statistical significance. *P* values from interaction tests are reported, and those < 0.05 are highlighted in bold. (B) Barplot of pCR rates by expression level of gene signatures with a significant test of interaction with arm. High and low expression were defined according to the median expression value of the signature across all baseline samples.
FRD, false discovery rate; OR, odds ratio; pCR, pathologic complete response.

64.0%-91.8%) and 62.0% (95% CI 49.7%-73.2%). Notably, 12 patients with e-pCR had residual disease at surgery, indicating that early tumor clearance does not perfectly predict final pCR. The 12 e-pCR patients with RD at surgery were classified as e-pCR transient, whereas the 45 e-pCR patients with pCR at surgery were classified as e-pCR sustained. We compared baseline gene signatures among four groups: e-pCR sustained, e-pCR transient, and the group with tumor cells detected on treatment biopsy but achieving pCR (early RD converting in pCR, called pCR) or not (sustained RD, called RD) at surgery, using multinomial logistic regression. In the CT arm, low expression of proliferation gene sets was significantly associated with e-pCR sustained status. Gene sets of mitochondrial oxidative metabolism (oxidative phosphorylation and complex I—IV) were downregulated in the e-pCR sustained group in both arms, whereas glycolysis was downregulated in this group in the CT/A arm only (Figure 3B and C). Iron intake instead was upregulated only in the e-pCR sustained group of the CT arm. Immunological signatures were expressed at significantly higher levels in both e-pCR sustained and e-pCR transient samples of the CT/A arm than in pCR and RD samples. In the CT arm, however, these signatures were higher in the two e-pCR groups and in the pCR samples compared with RD samples, although not statistically significant (Figure 3B and C). These results suggest that a low level of proliferation and metabolic rewiring is necessary for a rapid response to chemotherapy. When an ICI is added, however, many cancers with a lower level of proliferation and high immune infiltration also achieve an early-pCR. Instead, high immune infiltration at baseline appeared insufficient for an early response to chemotherapy alone.

On-treatment gene signatures associated with response

Assessing gene expression during treatment may provide insight into treatment-induced tumor and microenvironment remodeling. Hence, we evaluated the association of D1C2 gene signatures with pCR. It is important to underline that e-pCR patients were not evaluable in this analysis. At baseline, we found that metabolic signatures negatively associated with pCR in the CT/A arm dominated the only significant signatures predictive of response. However, at D1C2, we found that most signatures were positively associated with pCR in both treatment arms. These signatures were related to immune cell types and processes (Figure 4A). In addition, we found five signatures with a treatment-dependent association with pCR (interaction test $P < 0.05$, Figure 4A and B). For example, high expression of the glutamate transmembrane signature was associated with higher pCR rates in the CT arm, although not in the CT/A arm. High expression of the coenzyme Q10, estrogen

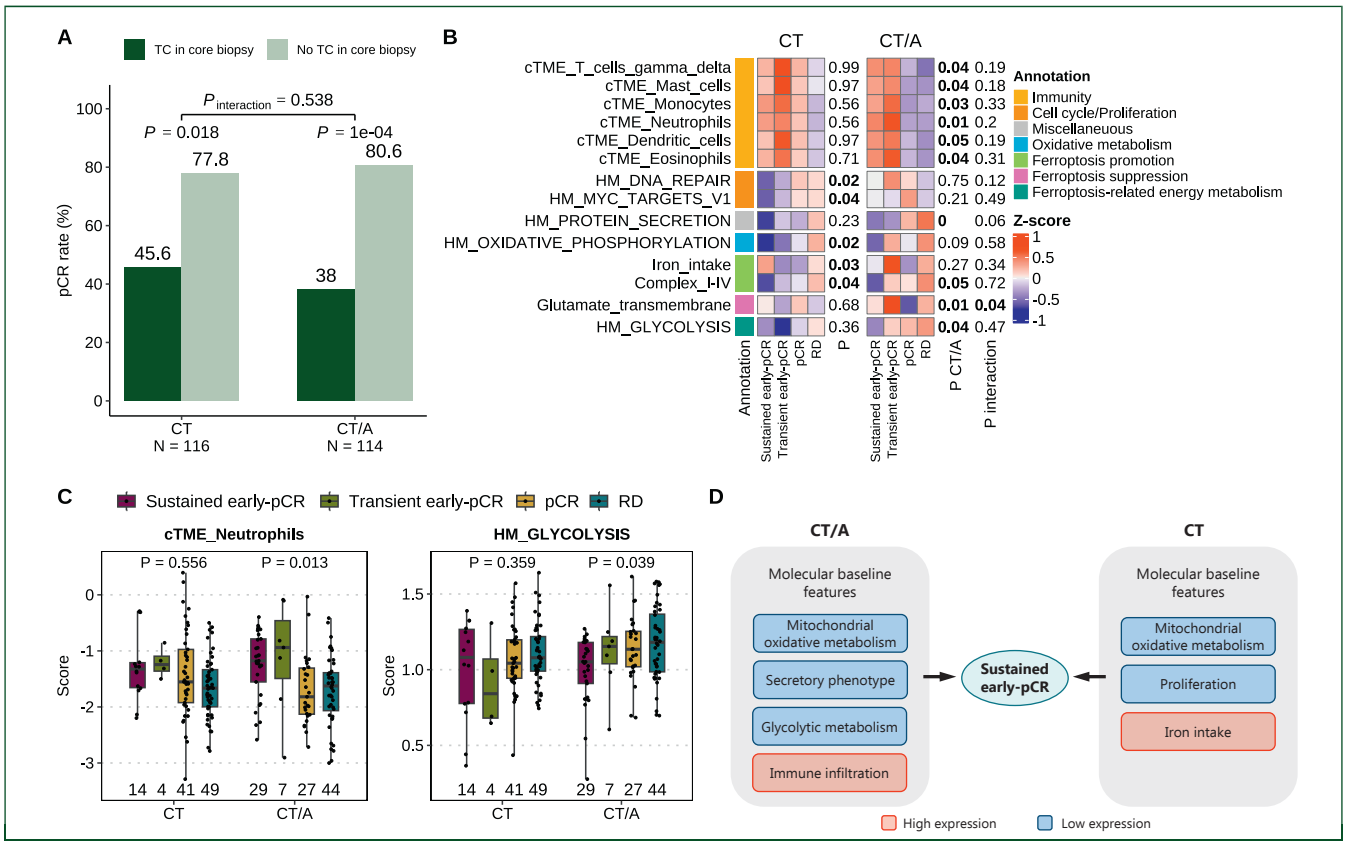

Figure 3. Baseline gene signatures associated with early response. (A) Barplot of pCR rates according to the presence or absence of tumor cells in the D1C2 core biopsy. (B) Heatmap of average gene signature *Z* scores according to the response group and treatment arm. Only gene signatures with a nominal *P* value < 0.05 according to multinomial logistic regression are reported. *P* values from interaction tests are reported. (C) Box plots showing the distribution of representative gene signatures according to the response group and treatment arm. *P* values of multinomial logistic regression are reported on top. (D) Schematic summary of the main baseline transcriptomic features of the e-pCR patients.
pCR, pathologic complete response.

response, apical surface, and hedgehog signaling signatures predicted a decreased pCR rate only in the CT arm. Two signatures, tetrahydrobiopterin (BH4) and the homocysteine metabolic process, were inversely associated with pCR rates in the CT/A arm, but not in the CT arm.

Together, these findings suggest that treatment dynamically reshapes the biological determinants of response, shifting from baseline metabolic features to therapy-induced immune activation, with distinct pathway dependencies emerging between treatment arms.

Treatment-induced transcriptional dynamics and association with pCR

Given that the timepoint is a known factor that significantly impacts expression profiles, and that the predictive biomarkers identified at baseline differ from those identified at D1C2, we examined the dynamics induced by treatment in 150 patients with paired baseline and D1C2 RNA-Seq data. Overall, we found that expression dynamics were similar in the two treatment arms. The major treatment-induced changes were related to an upregulation of immune and stromal signatures and to a downregulation of cell cycle signatures (Supplementary Figure S3A, available at https://doi.org/10.1016/j.annonc.2026.05.694). Metabolic signatures were heterogeneously modulated, with some being upregulated and others downregulated. At D1C2, carbohydrate metabolic signatures, oxidative phosphorylation, and most ferroptosis-suppressive pathways were downregulated. Ferroptosis induction signatures, mainly representing lipid and iron metabolism, were mostly upregulated at D1C2 (Supplementary Figure S3A, available at https://doi.org/10.1016/j.annonc.2026.05.694). Although the dynamics were similar between the two treatments, we found several signatures with significant interaction effects for the treatment arm. These signatures were predominantly immune-related and exhibited stronger upregulation in the CT/A arm than in the CT arm.

Next, we compared gene signatures between D1C2 and baseline, stratifying samples by treatment and pCR status (Supplementary Figure S3B, available at https://doi.org/10.1016/j.annonc.2026.05.694). We found that downregulation of proliferative signatures and upregulation of immune signatures at D1C2 were stronger in patients who achieved pCR than in those with RD. This was particularly evident in the CT/A arm, where the longitudinal modulation of most gene sets showed a statistically significant test of interaction between pCR and RD patients (Supplementary Figure S3B, available at https://doi.org/10.1016/j.annonc.2026.05.694).

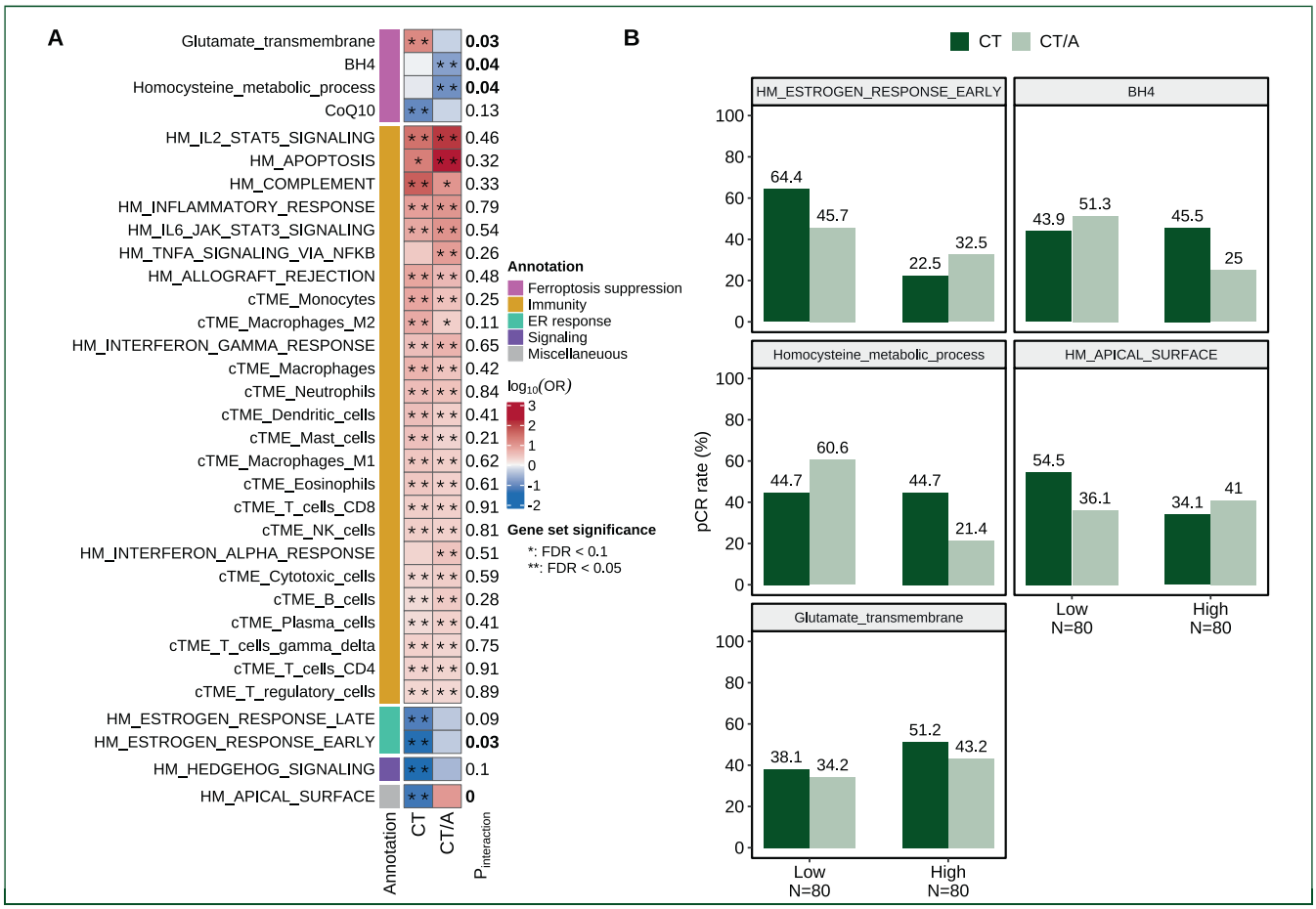

Figure 4. On-treatment gene signatures associated with pCR status. (A) The heatmap displays the log OR obtained from univariate logistic regression models. Gene signatures with an FDR < 0.05 in at least one treatment arm are reported. Asterisks indicate the level of statistical significance. *P* values from interaction tests are reported, and those < 0.05 are highlighted in bold. (B) Barplot of pCR rates by expression level of gene signatures with a significant test of interaction with arm. High and low expression was defined according to the median expression value of the signature across all D1C2 samples.
FDR, false discovery rate; OR, odds ratio; pCR, pathologic complete response.

To directly evaluate whether treatment-induced transcriptional changes were associated with pCR status, we performed a patient-level delta analysis by calculating the signature-wise expression difference between post- and pretreatment samples (Δ expression). We then compared Δ expression between pCR and RD using logistic regression. No significant association between Δ expression and pCR status was detected in the CT arm (Figure 5A). In the CT/A arm, many gene sets with a significant test of interaction in the differential expression analysis stratified by pCR status (Supplementary Figure S3B, available at https://doi.org/10.1016/j.annonc.2026.05.694) were also identified in the Δ analysis (Figure 5A), confirming that their treatment-induced regulation was specifically associated with response rather than representing a general pharmacodynamic effect. A negative Δ expression of cell cycle gene sets was associated with higher pCR rates, as well as a positive Δ expression of stromal (angiogenesis), immune, ferroptosis-promoting, and signaling (p53 and PI3K-AKT-MTOR) gene sets (Figure 5A). In particular, the HM_APICAL_SURFACE and HM_P53_PATHWAY gene sets showed an opposite association of their dynamics with pCR. Indeed, a higher Δ expression was associated with higher pCR rates in the CT/A arm, whereas a higher Δ expression was observed in the RD than in the pCR cases of the CT arm (Figure 5B).

We previously demonstrated that baseline TNBC subtypes predict response independently of whether immunotherapy is added to chemotherapy.[34] Here, we evaluated the dynamics of early TNBC subtypes and their association with response. We found that the most frequent TNBC subtype transitions from baseline to D1C2 were toward the immunomodulatory (IM) and mesenchymal stem-like subtypes (Supplementary Figure S4A, available at https://doi.org/10.1016/j.annonc.2026.05.694). This behavior aligns with the observed upregulation of immune and stromal signatures during treatment. On-treatment TNBC subtypes were similarly associated with pCR rates in the two treatment arms with the IM and luminal-androgen receptor subtypes being associated with the highest and lowest pCR rates, respectively (Supplementary Figure S4B, available at https://doi.org/10.1016/j.annonc.2026.05.694).

Together, these results indicate that neoadjuvant treatment drives a coordinated transcriptional reprogramming

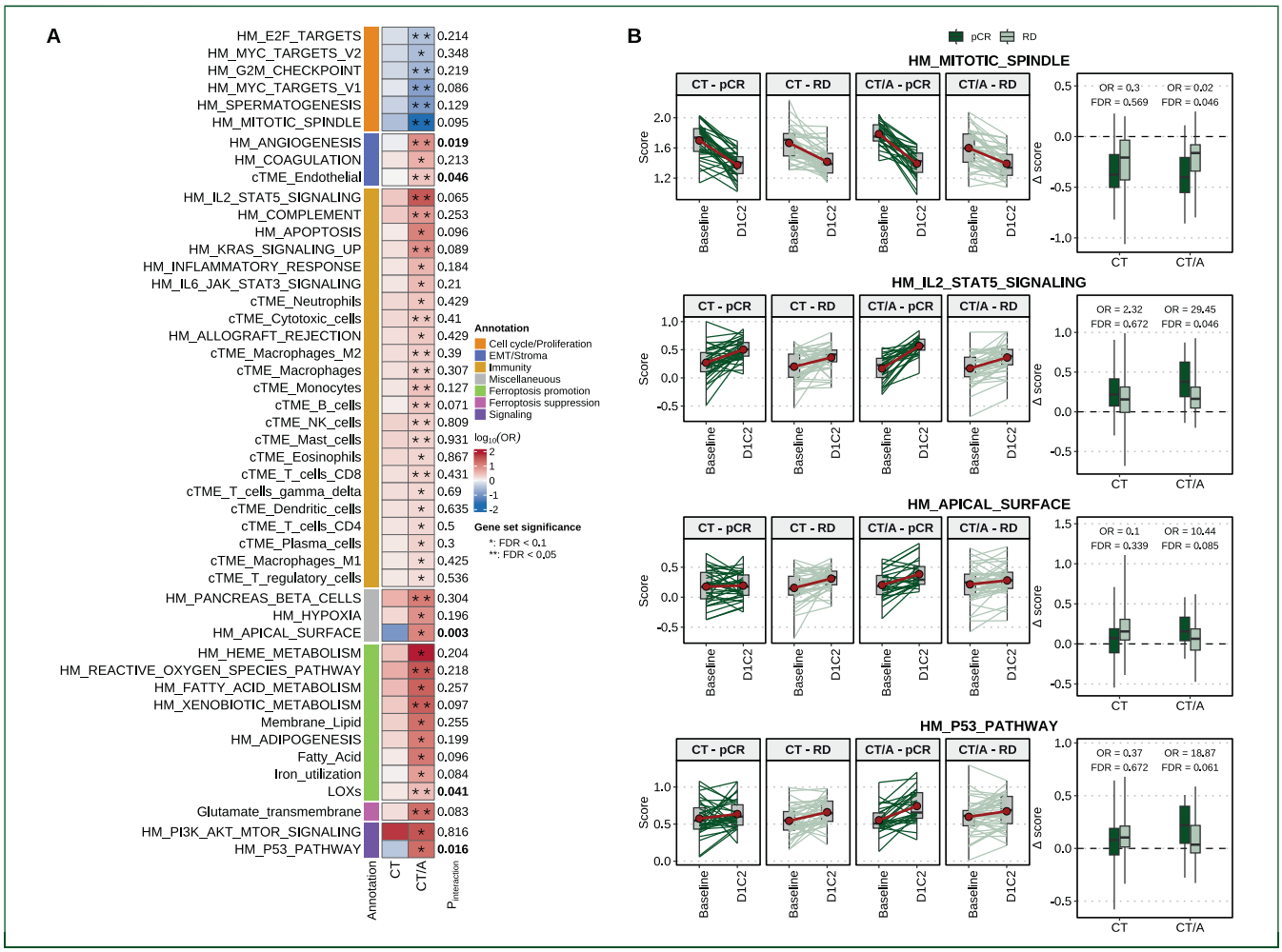

Figure 5. Longitudinal gene expression dynamics associated with treatment and response. (A) Heatmap of the log OR obtained from univariate logistic regression models for the D1C2 versus baseline Δ expression of variables. Gene signatures with an FDR < 0.05 in at least one treatment arm are reported. Asterisks indicate the level of statistical significance. *P* values from interaction tests are reported, and those < 0.05 are highlighted in bold. (B) Box plots of dynamic signatures during treatment. Lines represent gene signature dynamics in each patient. Red dots and lines represent the mean gene signature score for each class. For each signature, the boxplot of the distribution of Δ score by pCR status and treatment arm is shown.
FDR, false discovery rate; OR, odds ratio; pCR, pathologic complete response.

characterized by immune activation and proliferative arrest, especially in patients achieving pCR after chemoimmunotherapy.

Orthogonal immune deconvolution reveals dynamic cell-type–specific remodeling and association with pCR

To orthogonally validate the immune-related findings derived from ConsensusTME signatures, we performed bulk RNA-Seq deconvolution using InstaPrism to estimate immune cell fractions across timepoints.

We first assessed the concordance between cytotoxic tumor microenvironment (cTME) gene sets and inferred immune cell fractions. Strong and significant positive correlations were observed between corresponding signatures and deconvoluted cell types (Supplementary Figure S5A, available at https://doi.org/10.1016/j.annonc.2026.05.694), supporting the biological consistency between signature-based immune scores and quantitative cell fraction estimates. Poor cross-lineage correlations were observed, indicating the specificity of the deconvolution results.

We next examined immune cell proportions at baseline and at D1C2, stratified by treatment arm and pCR status. In the CT arm, baseline cell fractions were largely comparable across response groups. Indeed, no significant association between cell fraction and response was observed (Supplementary Figure S5B and C, available at https://doi.org/10.1016/j.annonc.2026.05.694). In the CT/A arm, a higher baseline proportion of T cells and a lower proportion of CAFs and normal cells were significantly associated with pCR (Supplementary Figure S5B and C, available at https://doi.org/10.1016/j.annonc.2026.05.694). In contrast, at D1C2, response-associated patterns emerged within both treatment arms. In both arms, pCR tumors displayed a significant increase in myeloid cells and a decrease in cancer epithelial cells. T and B cells were significantly associated with pCR in the CT/A and CT arm, respectively. A significant decrease of endothelial and normal epithelial cells was specifically observed in the CT arm (Supplementary Figure S5C, available at https://doi.org/10.1016/j.annonc.2026.05.694). The delta analysis of the cell

fractions (D1C2—baseline) showed a significant increase in myeloid cells and a decrease in cancer epithelial cells in pCR tumors compared with RD cases in the CT/A arm. Collectively, the deconvolution analysis recapitulates and extends the cTME-based findings, demonstrating that early treatment exposure induces measurable, cell-type—specific immune remodeling that is strongly associated with response.

Tumor purity-adjusted analysis distinguishes tumor-intrinsic transcriptional programs from microenvironment-driven signals

To assess the potential confounding effect of tumor purity in bulk RNA-Seq analyses, we evaluated the association of baseline and D1C2 gene signatures with pCR status adjusting the logistic regression models for InstaPrism tumor cellular composition.

At baseline, the association between gene expression and pCR remained consistent after adjustment for cellular composition, with comparable effect sizes and statistical significance observed in both adjusted and unadjusted models (Supplementary Figure S6A, available at https://doi.org/10.1016/j.annonc.2026.05.694).

In contrast, for on-treatment samples, although the direction and magnitude of the associations were largely preserved after adjustment, statistical significance was attenuated, suggesting a partial contribution of compositional effects to the observed signal (Supplementary Figure S6B, available at https://doi.org/10.1016/j.annonc.2026.05.694).

We further compared D1C2 versus pretreatment samples adjusting for tumor cellularity. Upon adjustment for cell-type fractions, most of the significant differences were markedly attenuated and no longer statistically significant. Notably, only a limited subset of gene signatures retained significance after adjustment. In particular, gene sets related to cell cycle and proliferation remained significantly downregulated independently of cellular composition (Supplementary Figure S6C, available at https://doi.org/10.1016/j.annonc.2026.05.694). This suggests that the suppression of proliferative programs represents a robust, cell-intrinsic effect of treatment, rather than a mere consequence of reduced tumor cellularity, supporting a direct impact of therapy on tumor cell cycling dynamics.

Overall, these results indicate that while a substantial proportion of the observed associations in on-treatment samples are driven by treatment-induced shifts in cellular composition, baseline predictors of response and the on-treatment suppression of proliferative programs remain robust after adjustment, supporting their interpretation as cell-intrinsic effects.

Multivariable modeling of gene signatures uncovers distinct predictors across treatments and timepoints

To explore the multivariable contribution of gene signatures to treatment response, we implemented an exploratory modeling framework based on XGBoost with repeated cross-validation. Importantly, this analysis was designed to evaluate the combined behavior and relative contribution of variables, rather than to derive a predictive model. For each arm, we trained three models using XGBoost, a machine learning algorithm that combines the predictions of many small decision trees, where each new tree learns to correct the errors made by the previous ones. The first model was trained using baseline data; the second, using D1C2 data; and the third, using a combination of the two timepoints' data. As previously mentioned, patients who achieved an e-pCR were not evaluable for the analyses of D1C2 and paired data. Cross-validated model accuracy was consistently higher in the CT/A arm than in the CT arm. For the CT/A arm, the baseline and D1C2 models achieved comparable accuracy. In contrast, D1C2 models outperformed baseline models in the CT arm (Figure 6A). Combining baseline and D1C2 data did not further improve performance in either the CT or CT/A arms (Figure 6A). Next, we sought to identify the most informative signatures by ranking them according to their median gain value, which is a measure of how much a feature improves the model's predictive capabilities. In the CT/A arm, both at baseline and D1C2, we observed a steep decrease in gain values after the top-two ranked features (Figure 6B). At baseline, the most important predictors of response to immunotherapy were the redox metabolic signature and the proliferative HM MITOTIC SPINDLE signature (Figure 6B).

In the D1C2 models, the cTME_Cytotoxic_cell and iron utilization signatures were consistently ranked among the most informative predictors (Figure 6B). To investigate the added value of combining relevant features, we performed partial dependence analysis, which shows the relationship between two variables and response in a trained regression model. We observed a clear combinatorial pattern of response probability when considering cTME_Cytotoxic_cell and iron utilization signatures together (Figure 6C). Although each variable individually stratified patients when dichotomized at the median, their joint modeling identified distinct regions of predicted probability, including areas enriched for high or low likelihood of pCR that were not apparent when evaluating each feature separately. This indicates that the relationship between cytotoxic immune activity and iron metabolism is not purely additive but reflects a more complex interaction in shaping treatment response.

Consistent with this observation, stratification of patients according to the categorical levels of the two variables demonstrated that their combination provided a clearer separation of response rates compared with either variable alone (Figure 6D). In particular, when cytotoxic T cell infiltration was low, iron utilization was not predictive of pCR status. However, with a high T cell infiltration iron utilization levels were associated with markedly different pCR rates, suggesting a potential interaction between immune cytotoxicity and tumor iron metabolism. Analysis of the gene expression dynamics of these two markers in the CT/A arm showed that

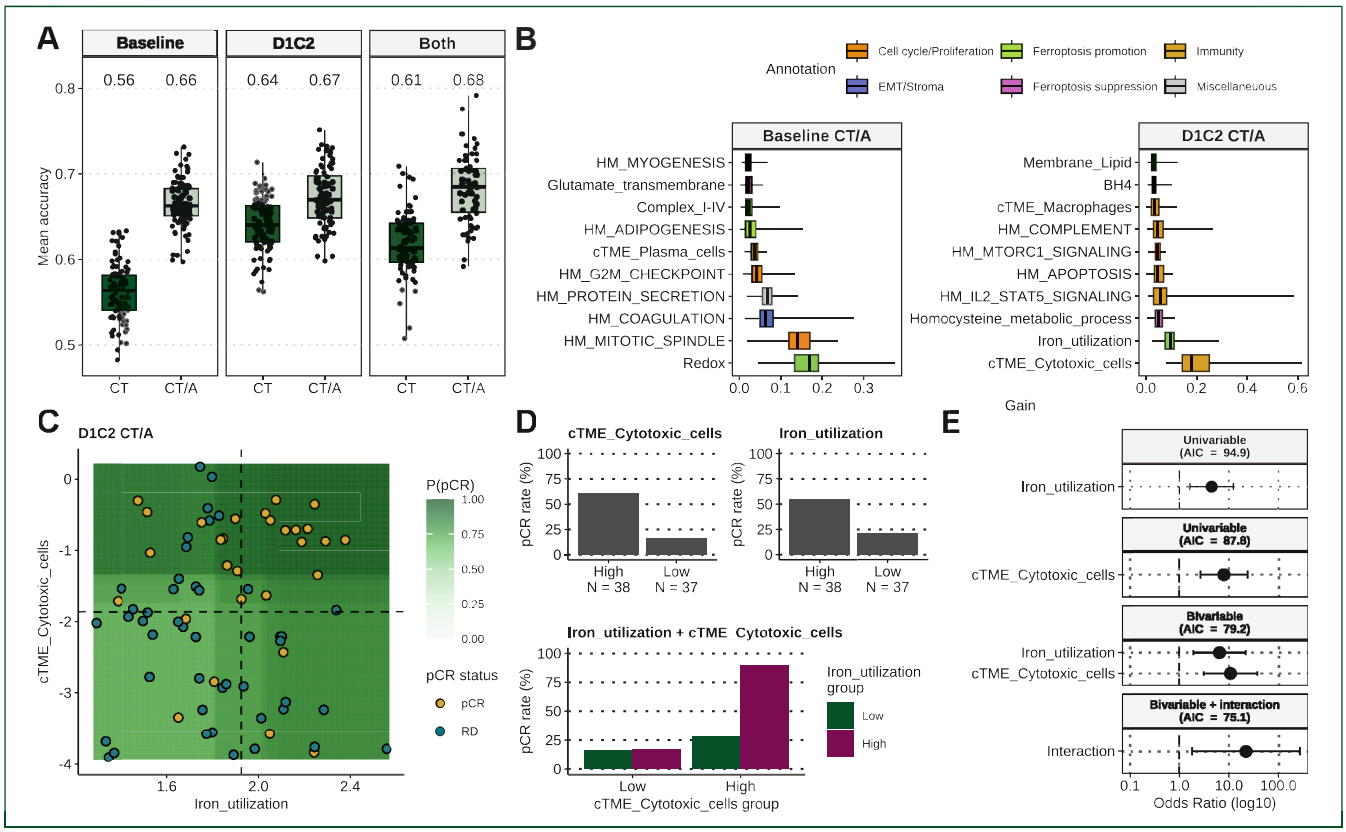

Figure 6. Multivariable models of treatment response. (A) Box plots of the mean cross-validated accuracies over the 100 iterations for XGBoost models trained to predict pCR status. Black points represent the mean cross-validated accuracy of a single iteration. (B) Box plots of mean gain values of the top-10 most important features for a given XGBoost model. (C) Partial dependence plot showing how the *joint variation* of the two predictors influences the model prediction. *X*- and *Y*-axes represent the gene signature expression scores. The green color gradient shows the change in predicted pCR probability according to the change in gene signature scores. Each dot represents a patient, colored by pCR status. Vertical and horizontal dashed lines represent the median expression score of the feature. (D) Bar plots showing the pCR rates according to immune cytotoxic activity and iron utilization. Upper panels show pCR rates stratified by the median value of each variable individually (cTME cytotoxic cells and iron utilization). Lower panels show pCR rates when combining the two dichotomized variables. (E) Forest plot summarizing the association between the categorized variables and pCR. OR and 95% confidence intervals are shown for univariable logistic regression models evaluating iron utilization and cTME cytotoxic cells individually, as well as for the multivariable model including both variables and their interaction term.
cTME, cytotoxic tumor microenvironment; OR, odds ratio; pCR, pathologic complete response.

the early on-treatment increase in iron utilization was observable only in patients achieving pCR and with a high cytotoxic T cell infiltration (Supplementary Figure S7, available at https://doi.org/10.1016/j.annonc.2026.05.694).

Finally, logistic regression models were used to provide a clinically interpretable quantification of these effects (Figure 6E). Although both variables showed significant associations with response in univariable analyses, their joint inclusion improved model fit, as reflected by a lower AIC. Moreover, the model including an interaction term further improved model fit, supporting the presence of a nonindependent relationship between the two features. Collectively, these analyses highlight the complementary and interacting contributions of cytotoxic immune infiltration and iron utilization to treatment response, illustrating how multivariable modeling can reveal patterns not captured by single-variable analyses.

DISCUSSION

By performing longitudinal transcriptomic profiling of TNBC before and during neoadjuvant treatment, this study provides a comprehensive view of how predictive biomarkers evolve under chemoimmunotherapy pressure. Notably, we found that baseline gene signatures had a stronger predictive value for neoadjuvant chemotherapy plus immunotherapy than for chemotherapy alone, suggesting that response to ICI/chemotherapy combination is more dependent on the treatment-naïve features of tumors. Baseline high expression of proliferation signatures and low expression of stromal and metabolic signatures were associated with pCR in patients receiving chemotherapy plus ICI. High expression of proliferation signatures at baseline is associated with pCR in several previous studies including patients receiving neoadjuvant chemotherapy or chemotherapy plus ICI combinations.[20,35,36] Using cell phenotyping, we previously showed that proliferation in several different cell types including cancer and immune cells mediates this association, which was particularly strong in the CT/A arm.[21] In contrast, high expression of gene signatures capturing epithelial-to-mesenchymal transition, angiogenesis, estrogen receptor signaling, and metabolic processes was associated with residual disease, with a stronger effect in the CT/A than in the CT arm. The association between stromal markers and lower sensitivity to

neoadjuvant ICI in TNBC has been previously reported[20,37-39] and may be mediated by cancer-associated fibroblasts and differentiated perivascular-like cells that can induce cytotoxic T cell dysfunction and exclusion.[37] Cancer-associated fibroblasts can also promote neo-angiogenesis,[37,38] which is inversely associated with $CD8^+$ cell infiltration in TNBC.[39] Metabolic pathways including fatty acid metabolism, cholesterol homeostasis, adipogenesis, oxidative phosphorylation, and glycolysis were also associated with RD in our study and in previous reports.[40] Gong et al.[41] proposed three metabolic-pathway—based TNBC classes, with the MPS1 class showing high lipid metabolism, enrichment in luminal-androgen receptor molecular subtype, and poor response to neoadjuvant chemotherapy and ICI. Lipid metabolic reprogramming and cholesterol biosynthesis also have immunosuppressive functions in the tumor microenvironment.[42] Hence, high expression of those metabolic pathways may be particularly relevant as a predictor of resistance to ICI and represent potential novel therapeutic targets. Both ferroptosis-inducing and ferroptosis-suppressive gene sets were found to be associated with a higher risk of RD in our cohort. This apparent paradox likely reflects the fact that these gene sets often capture a broader dysregulation of the pathway rather than its true functional activation or inhibition. Therefore, the association with RD is not driven by a specific functional direction of ferroptosis-related pathways, but rather by an overall dysregulation of ferroptosis-related metabolic programs in tumors that fail to achieve pCR.

Previous studies have shown that baseline immune signatures were predictive of neoadjuvant therapy in TNBC.[15,19,20,35,43,44] Furthermore, we previously demonstrated through imaging mass cytometry that immune cell phenotypes are associated with pCR in the NeoTRIP trial.[21] At the gene expression level, baseline immune signatures were positively associated with pCR rates but did not reach statistical significance after multiple testing correction. This relatively weak association between baseline immune presence and pCR after neoadjuvant chemotherapy in NeoTRIP, compared with the stronger associations seen in neoadjuvant trials that used anthracycline and taxane combinations, may be related to the lack of anthracyclines in the NeoTRIP regimen leading to a lesser chemotherapy-induced immune activation.[45,46]

Comparison of on-treatment with baseline tumors revealed a strong reduction of proliferation and an increase in immune and stromal markers in both treatment arms. This is consistent with DNA damage-induced cell cycle arrest that accompanies activation of DNA repair pathways in cancer cells, and with an acute inflammatory response that draws cytotoxic immune cells into the tumor microenvironment. These transcriptional changes are consistent with those observed in the longitudinal translational analysis of the GeparNuevo trial.[20]

In both arms, most metabolic signatures lost their predictive value when assessed on-treatment compared with baseline. Only two signatures, BH4 (tetrahydrobiopterin) and homocysteine metabolism, remained significantly associated with a higher risk of RD in the CT/A arm, suggesting that early on-treatment changes largely diminish the baseline metabolic signals. Although the mechanistic basis for these observations remains unclear, recently, it has been shown that GCH1, the rate-limiting enzyme of BH4 synthesis and a component of the BH4 signatures, promotes tumor growth and metastasis by driving epithelial-to-mesenchymal transition.[47] Therefore, these pathways may contribute to therapy resistance, although independent validation is warranted.

A high expression of immune signatures on-treatment was associated with a high probability of achieving pCR in both arms. However, the upregulation of immune signatures at D1C2 was stronger in the CT/A arm than the CT arm, especially in patients achieving pCR. This observation indicates that in the presence of an ICI added to chemotherapy, there is a stronger immune activation, which is linked to treatment response. Additionally, in our exploratory multivariable analyses of on-treatment features, the joint evaluation of cytotoxic T cell infiltration and iron utilization further highlighted a complementary contribution of immune and metabolic programs in shaping treatment response. Notably, their combined modeling identified response patterns that were not apparent when the two variables were considered individually, suggesting that interactions between immune cytotoxic activity and tumor metabolic states may influence sensitivity to therapy, with the effect of iron utilization emerging predominantly in tumors with high cytotoxic immune infiltration.

Importantly, bulk RNA-Seq does not allow discrimination between transcriptional changes occurring within tumor cells and shifts in cellular composition induced by treatment. The analyses repeated on tumor purity-adjusted expression data suggested that while baseline transcriptional differences associated with response were largely preserved, most immune associations found on-treatment were attenuated, indicating that part of the observed dynamics reflects treatment-induced reduction of tumor cellularity and remodeling of the tumor microenvironment rather than tumor-intrinsic transcriptional changes. These findings underscore that on-treatment transcriptional biomarkers capture both tumor-intrinsic responses and dynamic changes in tumor microenvironment composition.

In this context, cases with early-pCR (no tumor cells in on-treatment biopsy) represent an extreme manifestation of this process, where treatment-induced tumor depletion is so profound that no residual tumor cells are detectable. This early response was observed in both treatment arms, but it was significantly more common in the CT/A arm, suggesting that a rapid cytotoxic T cell response augments the direct cytotoxicity of chemotherapy. Indeed, early responders had the highest expression of immune signatures at baseline. Almost 80% of the patients who had no cancer in the early on-treatment biopsy (early-pCR) also had pCR at the time of surgery, which suggests that disappearance of tumor cells on D1C2 biopsy is a strong early surrogate of pCR at surgery.

Overall, this work demonstrated the relevance of collecting longitudinal samples in neoadjuvant trials and that

assessment of on-treatment biological features provides predictive information that is independent and complementary to baseline biological characteristics. This finding is consistent with previous studies on neoadjuvant therapy in this and other breast cancer subtypes.[21,48,49] The potential clinical applicability of baseline and on-treatment predictive information is different. Baseline biomarkers may be used to improve patient allocation by identifying those patients with the highest likelihood of responding to a given therapy, favoring other alternative treatments. On-treatment biomarkers, by contrast, capture the actual early biological response, which might be used to guide response-adapted strategies, such as early treatment change to alternative treatment options or in case of optimal response try to de-escalate treatments by offering for instance shorter treatment exposure.

This concept of adapting neoadjuvant therapy based on early indicators of treatment response is gaining interest in the treatment of early breast cancer. Building on the adaptive trial I-SPY 2,[43] the ongoing I-SPY 2.2 trial implemented a strategy in which treatment is dynamically adapted to the actual predicted probability of achieving a pCR or not responding to treatment, instead of administering a predefined sequence and duration of treatment.[50,51] In this design, early on-treatment assessments, including MRI imaging and tumor biopsies, guide the anticipation of surgery for patients highly likely to achieve a pCR. For patients not responding after two cycles of treatment, an early change of therapy is offered. The goal of this strategy is to improve outcomes while minimizing unnecessary treatment exposure.

In this scenario, our work provided supportive evidence that integrating molecular profiling both before and early on-treatment could contribute to inform personalized treatment strategies in TNBC.

Our analysis has limitations. As previously discussed, transcriptomic profiling by bulk RNA-Seq averages out gene expression signals across all cell types in a sample. This could mask biologically relevant variation arising from rare cellular subpopulations within the tumor microenvironment. This limitation may be overcome by emerging technologies such as single-cell RNA-Seq and spatial transcriptomics or proteomics, which enable higher-resolution characterization of tumor and immune cell states and their spatial organization within the tumor microenvironment. However, these approaches currently require complex experimental workflows, higher tissue input, and substantial analytical resources, which limit their scalability and routine implementation in large clinical trials or in real-world clinical settings. In this context, bulk RNA-Seq remains a practical and robust strategy for biomarker discovery in large neoadjuvant studies, particularly when coupled with computational approaches aimed at deconvolving cell-type composition or capturing immune-related transcriptional programs. Furthermore, analysis of on-treatment samples inevitably excluded patients with an early response, due to the absence of detectable tumor cells and corresponding RNA-Seq data. This may have introduced selection bias when assessing the association between on-treatment gene signatures and response. Patients with early-pCR (e-pCR) were necessarily excluded from on-treatment (D1C2) and paired analyses due to the absence of detectable tumor cells and corresponding RNA-Seq data. Consequently, these analyses are enriched for tumors that are not highly responsive to therapy, and our results on on-treatment immune and stromal signatures should be interpreted in this context.

The absence of an independent dataset of on-treatment biopsies from TNBC patients undergoing neoadjuvant chemoimmunotherapy prevented us from externally validating our findings. Finally, event-free survival data were not available for the analyses, but it is well established that patients who achieve a pCR have excellent long-term survival, especially in TNBC.[52] Therefore, predicting whether an individual has a higher chance of achieving this outcome when treated with an ICI is accepted as a valid surrogate for translational research.[52] In future studies, gene expression signatures will be assessed as predictors of event-free survival.

Despite these limitations, our study provides a broad comprehensive evaluation of the temporal transcriptomic dynamics and their association with response to neoadjuvant chemotherapy with and without atezolizumab in TNBC patients. Assessing longitudinal biomarkers could provide clinicians with a framework in which on one side baseline biomarkers could help select patients for optimal treatment, and on the other side, on-treatment biomarkers could help adjust treatment according to the tumor's adaptive response. In summary, this study establishes a foundation for future investigations into dynamic biomarkers of response, which may ultimately guide the personalization and optimization of neoadjuvant chemoimmunotherapy in TNBC.

FUNDING

This work was supported by Fondazione AIRC per la Ricerca sul Cancro (grants IG 2018 — 21787, IG 2024 to G. Bianchini), the Breast Cancer Research Foundation (BCRF; grant 18-181, 20-181 to L. Gianni), and unrestricted grants from Insight Molecular Diagnostics, TN, USA (no grant number applicable). The NeoTRIPaPDL1 trial was supported by Fondazione Michelangelo, Milan, Italy; by unrestricted grants and free study drugs from Hoffman-La Roche Ltd, Switzerland; and by Celgene, a Bristol-Myers Squibb Company, Switzerland. G. Bianchini is also supported by a donation from Carmelina Ratto and Carlo Capra.

DISCLOSURE

MD has received travel support from Insight Molecular Diagnostics. C-SH has received research grants for his institution from Aston Sci, AstraZeneca, Daiichi Sankyo, EirGenix, Eli Lilly, Gilead, MSD, Novartis, OBI Pharma, Pfizer, Roche and Seagen; honoraria for speakers' bureaus from AstraZeneca, Daiichi Sankyo, Eli Lilly, Novartis, Pfizer, and Roche; support for attending meetings from Pfizer; and has served on advisory boards for AstraZeneca, Daiichi Sankyo, Eli Lilly, Novartis, Pfizer and Roche. DE has received consulting fees

from AstraZeneca, Daichii Sankyo, Gilead, Novartis, MSD, Roche, Pfizer and Seagen; honoraria for lectures from Amgen, AstraZeneca, Daichii Sankyo, Novartis, MSD, Roche and Pfizer; and support for attending meetings from Pfizer and Roche. BB has received honoraria for speaker bureaus from MDS, Roche, Novartis, Pfizer, Palex, AstraZeneca and Lilly; and has served on advisory boards for MSD, Roche and Daichii Sankyo. RSS receives compensation from Insight Molecular Diagnostics. TJN is an employee of Insight Molecular Diagnostics. CZ has received grants from Eisai, Pharmamar, Eli Lilly, Celgene, MSD, GSK, Amgen and Daichii Sankyo, and for him and his institution from Roche, Novartis, AstraZeneca, Pfizer, Tesaro, Pierre Fabre, Ist. Gentili, Teva and Seagen; support for attending meetings from Roche, Novartis, Pfizer, Pharmamar, Tesaro, Pierre Fabre, Ist. Gentili and Celgene; has served on advisory boards for Roche, Eisai, Novartis, AstraZeneca, Pfizer, Pharmamar, Amgen, Tesaro, QuintilesIMS, Eli Lilly, Celgene, MSD, GSK and Daichii Sankyo; and has received other financial and nonfinancial interests from Roche, Novartis, AstraZeneca, Pfizer, Amgen, Tesaro, QuintilesIMS, MSD, GSK and Daichii Sankyo. MT has served on advisory boards for Agendia, Amgen, AstraZeneca, Aurikamed, Becton/Dickinson, ClearCut, Daiichi Sankyo, Exact Sciences, Gilead Science, GSK, Hexal, Lilly, MSD, Novartis, Onkowissen, Pfizer, pfm Medical, Roche, Saman Tree, Seagen, Sirius Medical, Sysmex, Titanium Textiles; has received manuscript support from Amgen, Cairn Surgical, ClearCut, pfm Medical, Servier; has received travel support from Amgen, Art Tempi, AstraZeneca, Clearcut, Daiichi Sankyo, Exact Sciences, Gilead, Hexal, I-Med-Institute, Lilly, Menarini Stemline, MSD, Neodynamics, Novartis, Pfizer, pfm Medical, Roche, RTI Surgical, Seagen, Zuellig Pharma; has received support for attending meetings from Amgen, AstraZeneca, Daiichi Sanyko, Gilead, Hexal, Lilly, Menarini Stemline, Novartis, Pfizer, pfm Medical, Roche, Sirius Medical; has received lecture honoraria from Agendia, Amgen, Art Tempi, AstraZeneca, Endomag, Exact Sciences, Gilead Science, GSK, Hexal, I-Med-Institute, Jörg Eickeler, Johnson and Johnson, Laborarztpraxis Walther et al., Lilly, Medscape, Menarini Stemline, MSD, Novartis, Onkowissen, Pfizer, pfm Medical, Roche, Seagen, Sirius Medical, StreamedUp, Sysmex, Zuellig Pharma; has received trial funding from Endomag, Exact Sciences; has received trial honoraria from AstraZeneca, CairnSurgical, Clearcut, Novartis, Novus Scientific, pfm Medical, Roche, RTI Surgical. AA-T has received consulting fees from Daichii Sankyo, Roche, Pfizer, and Bayer Spain; payment for expert testimony from Pfizer; has served on Advisory Boards for Lilly and Gilead; and has received other services from GSK. ES reports grants from Roche, MSD and BMS; honoraria from Roche, Janssen, MSD and BMS; travel/meeting expenses Roche and Pfizer; consulting fees from Roche; participation on a data safety monitoring board/advisory board for Roche; leadership/fiduciary role in other board for Roche. EMC has received consulting fees from Roche, Lilly, AstraZeneca, Daiichi Sankyo, Novartis, Pfizer, and MSD; honoraria for speakers' bureaus from Lilly and Roche; and support for attending meetings from Pfizer and Roche. BLS is an employee of Insight Molecular Diagnostics. RG has received consulting fees from Celgene, Novartis, Roche, BMS, Takeda, Abbvie, AstraZeneca, Jaanssen, MSD, Merk, Gilead, Daiichi Sankyo and Sanofi; support for attending meetings from Roche, Amgen, Janssen, AstraZeneca, Novartis, MSD, Celgene, Gilead, BMS, Abbvie and Daiichi Sankyo; has served on Advisory Boards for Celgene, Novartis, Roche, BMS, Takeda, Abbvie, AstraZeneca, Jaanssen, MSD, Merk, Gilead, Daiichi Sankyo and Sanofi; and has received other financial or nonfinancial interests from Celgene, Roche, Merk, Takeda, AstraZeneca, Novartis, Amgen, BMS, MSD, Sandoz, Abbvie, Gilead, Daiichi Sankyo, Eli Lilly and Novo Nordisk. MC has received a research grant from Roche. CMK has received grants from the Mater Foundation and HRB Grant/Hospital Co investment and from the Irish Cancer Society; honoraria for educational events from Exact Sciences, AstraZeneca, and Daiichi Sankyo; support for attending meetings from Roche; and has participated in Steering Committees for the PALLAS trial, the PenelopeB trial and Destiny Breast 11. LDM has received honoraria for speakers' bureaus from Roche, Novartis, Eli Lilly, MDS, Pfizer, Ipsen and from Novartis for her institution; support for attending meetings from Roche, Pfizer, Celgene, AstraZeneca, and Daiichi Sankyo; and has served on advisory boards for Roche, Eli Lilly, Novartis, MSD, Pfizer, Genomic Health, Pierre Fabre, Daiichi Sankyo, Seagen, Gilead, Exact Sciences, GSK and Agendia. GiV has received travel support from Eli Lilly, Pfizer, and AstraZeneca; has served on advisory boards for Pfizer and Novartis; has received speaker honoraria from Daichii Sankyo and Eli Lilly. LP has stock and other ownership Interests with Ataraxis; has received honoraria from Natera, Merck and Co, Radionetics, Agendia, AstraZeneca, Bristol Myers Squibb; has received consulting or advisory board fees from Merck, AstraZeneca, Bristol Myers Squibb, Agendia, Radionetics, Natera, Personalis; has received research fundings for his institution from Merck, AstraZeneca, Bristol Myers Squibb, Pfizer, Menarini, Natera, Exact Sciences, Personalis, Agendia. GV has received research supports from Roche-Genentech, Ventana Medical Systems, Dako-Agilent Technologies; has received honoraria or consultation fees from Dako-Agilent Technologies, Roche, MSD Oncology, AstraZeneca, Daiichi Sankyo, Pfizer, Eli Lilly, and Gilead. LG has received consulting fees from Novartis and Odonate Therapeutics; honoraria for lectures from Roche; and support for attending meetings from Pfizer; is co-inventor of 'European Patent Application Nos. 12195182.6 and 12196177.5 titled PDL-1 expression in anti-HER2 therapy'—Roche—Issued (no compensation provided); has served on advisory boards for AstraZeneca, Celgene, Genentech, Merk Sharp & Dohme, Roche, Pfizer and Sanofi Aventis; and is Chair of the Breast Cancer Research Committee of Fondazione Michelangelo. GB has received consulting fees from Roche, AstraZeneca, Novartis, MSD, Sanofi, Daiichi Sankyo, and Exact Science; honoraria for speakers' bureaus from Roche, Pfizer, AstraZeneca, Lilly, Novartis, Neopharm Israel, MSD, Chugai, Daiichi Sankyo, EISAI, and Exact Science; support for attending meetings from Roche, Pfizer, and AstraZeneca; and has served on advisory boards for Roche, Pfizer, Daiichi Sankyo, Lilly, MSD,

Novartis, AstraZeneca, Genomic Health, EISAI, Gilead and Seagen. All remaining authors have declared no conflicts of interest.

REFERENCES

1. Bianchini G, De Angelis C, Licata L, Gianni L. Treatment landscape of triple-negative breast cancer—expanded options, evolving needs. *Nat Rev Clin Oncol*. 2022;19(2):91-113.
2. Stanton SE, Adams S, Disis ML. Variation in the incidence and magnitude of tumor-infiltrating lymphocytes in breast cancer subtypes: a systematic review. *JAMA Oncol*. 2016;2:1354-1360.
3. Loizides S, Constantinidou A. Triple negative breast cancer: immunogenicity, tumor microenvironment, and immunotherapy. *Front Genet*. 2023;13:1095839.
4. Ali HR, Glont SE, Blows FM, et al. PD-L1 protein expression in breast cancer is rare, enriched in basal-like tumours and associated with infiltrating lymphocytes. *Ann Oncol*. 2015;26:1488-1493.
5. Buisseret L, Garaud S, de Wind A, et al. Tumor-infiltrating lymphocyte composition, organization and PD-1/PD-L1 expression are linked in breast cancer. *Oncoimmunology*. 2017;6:e1257452.
6. Schmid P, Cortes J, Pusztai L, et al. Pembrolizumab for early triple-negative breast cancer. *N Eng J Med*. 2020;382:810-821.
7. Schmid P, Cortes J, Dent R, et al. Event-free survival with pembrolizumab in early triple-negative breast cancer. *N Engl J Med*. 2022;386:556-567.
8. Loibl S, Untch M, Burchardi N, et al. A randomised phase II study investigating durvalumab in addition to an anthracycline taxane-based neoadjuvant therapy in early triple-negative breast cancer: clinical results and biomarker analysis of GeparNuevo study. *Ann Oncol*. 2019;30:1279-1288.
9. Loibl S, Schneeweiss A, Huober J, et al. Neoadjuvant durvalumab improves survival in early triple-negative breast cancer independent of pathological complete response. *Ann Oncol*. 2022;33:1149-1158.
10. Nanda R, Liu MC, Yau C, et al. Effect of pembrolizumab plus neoadjuvant chemotherapy on pathologic complete response in women with early-stage breast cancer: an analysis of the ongoing phase 2 adaptively randomized I-SPY2 trial. *JAMA Oncol*. 2020;6:676-684.
11. Mittendorf EA, Zhang H, Barrios CH, et al. Neoadjuvant atezolizumab in combination with sequential nab-paclitaxel and anthracycline-based chemotherapy versus placebo and chemotherapy in patients with early-stage triple-negative breast cancer (IMpassion031): a randomised, double-blind, phase 3 trial. *Lancet*. 2020;396:1090-1100.
12. Schmid P, Cortés J, Dent RA, et al. LBA18 Pembrolizumab or placebo plus chemotherapy followed by pembrolizumab or placebo for early-stage TNBC: updated EFS results from the phase III KEYNOTE-522 study. *Ann Oncol*. 2023;34:S1257.
13. Loi S, Schmid P, Aktan G, Karantza V, Salgado R. Relationship between tumor infiltrating lymphocytes (TILs) and response to pembrolizumab (pembro)+chemotherapy (CT) as neoadjuvant treatment (NAT) for triple-negative breast cancer (TNBC): phase Ib KEYNOTE-173 trial. *Ann Oncol*. 2019;30:iii2.
14. Bianchini G, Huang CS, Egle D, et al. LBA13 Tumour infiltrating lymphocytes (TILs), PD-L1 expression and their dynamics in the NeoTRIPaPDL1 trial. *Ann Oncol*. 2020;31:S1145-S1146.
15. Sinn BV, Loibl S, Hanusch CA, et al. Immune-related gene expression predicts response to neoadjuvant chemotherapy but not additional benefit from PD-L1 inhibition in women with early triple-negative breast cancer. *Clin Cancer Res*. 2021;27:2584-2591.
16. Mittempergher L, Kuilman MM, Barcaru A, et al. The ImPrint immune signature to identify patients with high-risk early breast cancer who may benefit from PD1 checkpoint inhibition in I-SPY2. *JCO*. 2022;40:514. 514.
17. Virassamy B, Caramia F, Savas P, et al. Intratumoral CD8+ T cells with a tissue-resident memory phenotype mediate local immunity and immune checkpoint responses in breast cancer. *Cancer Cell*. 2023;41:585-601.e8.
18. Iwase T, Blenman KRM, Li X, et al. A novel immunomodulatory 27-gene signature to predict response to neoadjuvant immunochemotherapy for primary triple-negative breast cancer. *Cancers*. 2021;13:4839.
19. Karn T, Denkert C, Weber KE, et al. Tumor mutational burden and immune infiltration as independent predictors of response to neoadjuvant immune checkpoint inhibition in early TNBC in GeparNuevo. *Ann Oncol*. 2020;31:1216-1222.
20. Denkert C, Schneeweiss A, Rey J, et al. Molecular adaptation to neoadjuvant immunotherapy in triple-negative breast cancer. *Cell Rep Med*. 2024;5:101825.
21. Wang XQ, Danenberg E, Huang CS, et al. Spatial predictors of immunotherapy response in triple-negative breast cancer. *Nature*. 2023;621:868-876.
22. Shiao SL, Gouin KH, Ing N, et al. Single-cell and spatial profiling identify three response trajectories to pembrolizumab and radiation therapy in triple negative breast cancer. *Cancer Cell*. 2024;42:70-84.e8.
23. Dugo M, Huang CS, Egle D, et al. Abstract P2-07-12: Triple negative breast cancer subtypes and early dynamics of the 27-gene IO score predict pCR in the NeoTRIPaPDL1 trial. *Cancer Res*. 2022;82:P2-07—12.
24. Gianni L, Huang CS, Egle D, et al. Pathologic complete response (pCR) to neoadjuvant treatment with or without atezolizumab in triple-negative, early high-risk and locally advanced breast cancer: NeoTRIP Michelangelo randomized study. *Ann Oncol*. 2022;33:534-543.
25. Dobin A, Davis CA, Schlesinger F, et al. STAR: ultrafast universal RNA-seq aligner. *Bioinformatics*. 2013;29:15-21.
26. Li B, Dewey CN. RSEM: accurate transcript quantification from RNA-Seq data with or without a reference genome. *BMC Bioinformatics*. 2011;12:323.
27. Liberzon A, Birger C, Thorvaldsdóttir H, Ghandi M, Mesirov JP, Tamayo P. The molecular signatures database hallmark gene set collection. *Cell Systems*. 2015;1:417-425.
28. Jiménez-Sánchez A, Cast O, Miller ML. Comprehensive benchmarking and integration of tumor microenvironment cell estimation methods. *Cancer Res*. 2019;79:6238-6246.
29. Yang F, Xiao Y, Ding JH, et al. Ferroptosis heterogeneity in triple-negative breast cancer reveals an innovative immunotherapy combination strategy. *Cell Metab*. 2023;35:84-100.e8.
30. Ritchie ME, Phipson B, Wu D, et al. limma powers differential expression analyses for RNA-sequencing and microarray studies. *Nucleic Acids Res*. 2015;43:e47. e47.
31. Hu M, Chikina M. InstaPrism: an R package for fast implementation of BayesPrism. *Bioinformatics*. 2024;40:btae440.
32. Chen T, Guestrin C. XGBoost: a scalable tree boosting system. In: *Proceedings of the 22nd ACM SIGKDD International Conference on Knowledge Discovery and Data Mining*. New York, NY: Association for Computing Machinery. p. 785-794. Available at https://dl.acm.org/doi/10.1145/2939672.2939785; 2016.
33. Hu L, Hu J, Qin C, Liu S, Yu Y. Ferroptosis in TNBC: interplay with tumor-infiltrating immune cells and therapeutic implications. *Mol Cell Biochem*. 2025;480:5029-5039.
34. Dugo M, Huang CS, Egle D, et al. The immune-related 27-gene signature determines response to neoadjuvant atezolizumab plus chemotherapy in triple-negative breast cancer. *Clin Cancer Res*. 2024;30:4900-4909.
35. Blenman KRM, Marczyk M, Karn T, et al. Predictive markers of response to neoadjuvant durvalumab with nab-paclitaxel and dose-dense doxorubicin/cyclophosphamide in basal-like triple-negative breast cancer. *Clin Cancer Res*. 2022;28:2587-2597.
36. Filho OM, Stover DG, Asad S, et al. Association of immunophenotype with pathologic complete response to neoadjuvant chemotherapy for triple-negative breast cancer: a secondary analysis of the BrighTNess phase 3 randomized clinical trial. *JAMA Oncol*. 2021;7:603-608.
37. Wu SZ, Roden DL, Wang C, et al. Stromal cell diversity associated with immune evasion in human triple-negative breast cancer. *EMBO J*. 2020;39:e104063.
38. Wang FT, Sun W, Zhang JT, Fan YZ. Cancer-associated fibroblast regulation of tumor neo-angiogenesis as a therapeutic target in cancer. *Oncol Lett*. 2019;17:3055-3065.
39. Wu SY, Xu Y, Chen L, et al. Combined angiogenesis and PD-1 inhibition for immunomodulatory TNBC: concept exploration and biomarker analysis in the FUTURE-C-Plus trial. *Mol Cancer*. 2022;21:84.

40. Anurag M, Jaehnig EJ, Krug K, et al. Proteogenomic markers of chemotherapy resistance and response in triple-negative breast cancer. *Cancer Discov*. 2022;12:2586-2605.
41. Gong Y, Ji P, Yang YS, et al. Metabolic-pathway-based subtyping of triple-negative breast cancer reveals potential therapeutic targets. *Cell Metab*. 2021;33:51-64.e9.
42. Zheng M, Zhang W, Chen X, et al. The impact of lipids on the cancer—immunity cycle and strategies for modulating lipid metabolism to improve cancer immunotherapy. *Acta Pharm Sin B*. 2023;13:1488-1497.
43. Wolf DM, Yau C, Wulfkuhle J, et al. Redefining breast cancer subtypes to guide treatment prioritization and maximize response: predictive biomarkers across 10 cancer therapies. *Cancer Cell*. 2022;40:609-623.e6.
44. Loibl S, Sinn B, Karn T, et al. Abstract PD2-07: mRNA signatures predict response to durvalumab therapy in triple negative breast cancer (TNBC)—results of the translational biomarker programme of the neoadjuvant double-blind placebo controlled GeparNuevo trial. *Cancer Res*. 2019;79:PD2-07.
45. Galluzzi L, Humeau J, Buqué A, Zitvogel L, Kroemer G. Immunostimulation with chemotherapy in the era of immune checkpoint inhibitors. *Nat Rev Clin Oncol*. 2020;17:725-741.
46. Callari M, Barreca M, Dugo M, et al. Abstract PD10-09: Comparison of early modulation of biological pathways and immune microenvironment by anthracyclines- or taxane-based treatment. *Cancer Res*. 2022;82:PD10-09.
47. Wang Z, Zhang N, Zhang M, et al. GTP cyclohydrolase drives breast cancer development and promotes EMT in an Enzyme-independent manner. *Cancer Res*. 2023;83:3400-3413.
48. Bownes RJ, Turnbull AK, Martinez-Perez C, Cameron DA, Sims AH, Oikonomidou O. On-treatment biomarkers can improve prediction of response to neoadjuvant chemotherapy in breast cancer. *Breast Cancer Res*. 2019;21:73.
49. Turnbull AK, Arthur LM, Renshaw L, et al. Accurate prediction and validation of response to endocrine therapy in breast cancer. *J Clin Oncol*. 2015;33:2270-2278.
50. Shatsky RA, Trivedi MS, Yau C, et al. Datopotamab—deruxtecan plus durvalumab in early-stage breast cancer: the sequential multiple assignment randomized I-SPY2.2 phase 2 trial. *Nat Med*. 2024;30:3737-3747.
51. Khoury K, Meisel JL, Yau C, et al. Datopotamab—deruxtecan in early-stage breast cancer: the sequential multiple assignment randomized I-SPY2.2 phase 2 trial. *Nat Med*. 2024;30:3728-3736.
52. Huang M, O'Shaughnessy J, Zhao J, et al. Association of pathologic complete response with long-term survival outcomes in triple-negative breast cancer: a meta-analysis. *Cancer Res*. 2020;80:5427-5434.